Applied Water Science (2023) 13:226
https://doi.org/10.1007/s13201-023-02034-w

ORIGINAL ARTICLE

Zinc chloride activated carbon derived from date pits for efficient biosorption of brilliant green: adsorption characteristics and mechanism study

Magda A. Akl[1] · Aya G. Mostafa[1] · Mohammed Al-Awadhi[2] · Wegdan S. Al-Harwi[3] · Abdelrahman S. El-Zeny[1]

Received: 22 June 2023 / Accepted: 16 October 2023 / Published online: 4 November 2023

Abstract

It is critical to remove dyes from wastewater as they cause harm to human and aquatic life due to their carcinogenic, toxic, and mutagenic effects. Here, low-cost activated carbons (CPs) were produced from the date (*Phoenix dactylifera* L.) pits. The prepared CPs were chemically activated utilizing zinc chloride to obtain activated carbons from date pits (ZCPs). The physicochemical properties, chemical composition, and morphology of ZCPs material and the active surface functional groups involved in adsorption were identified using N_2 adsorption–desorption isotherm, scanning electron microscopy, point of zero charges (pH_{PZC}), and Fourier transforms spectroscopy. The ZCPs biocomposite was applied for the Brilliant green (BG) removal from aqueous solutions, where the efficiency was assessed as functions of pH value, foreign ions, the initial dye concentration, dose of adsorbent, adsorption time, and temperature. The outcomes showed that the prepared ZCPs biocomposite exhibited high uptake of BG with a q_e of 247.752 mg/g. The isotherm and kinetic studies show that the adsorption process of BG dye onto ZCPs biocomposite followed Langmuir, and pseudo-second-order models, respectively. From the estimated thermodynamic functions, it was found that the nature of the BG dye adsorption process onto the prepared ZCPs adsorbent was endothermic and spontaneous. With a relative standard deviation of less than 3%, the prepared ZCPs were successfully applied for the removal of BG from real water samples with a recovery of more than 90%. The plausible mechanism of BG adsorption onto the prepared ZCPs can be assigned to various interactions, such as pore–filling, electrostatic attraction, H-bonding, and π–π stacking.

Keywords Date (*Phoenix dactylifera* L.) pits · Activated carbon · Brilliant green · Adsorption · Isotherms

Introduction

As dyes are employed in several industries such as printing, pharmaceutical, plastic, and fabrics, their effluents are discharged into water bodies and may harm human and aquatic life beings due to their carcinogenic, toxic, and mutagenic effects (Mostafa et al. 2023; Abd-Elhamid et al. 2020; Ibrahim et al. 2019; Behera et al. 2017; Youssef et al. 2016; Nandi et al. 2009).

✉ Magda A. Akl
magdaakl@yahoo.com

[1] Department of Chemistry, Faculty of Science, Mansoura University, Mansoura 35516, Egypt

[2] Department of Chemistry, Faculty of Education and Science, Saba Region University, Marib, Yemen

[3] Faculty of Science, University of Zawia, Zawia, Libya

Brilliant green (BG) is a derivative of triarylmethane dye. It is employed in various medical applications as it can be used as a veterinary drug, a biological stain, a dermatological agent, and an antimold. It is also used in different industries like printing and paper and fabric dying. BG dye is dangerous in case of skin contact, eye contact, and swallowing. It is toxic to the lungs, through inhalation. During its degradation, it produces CO_2, NO, and sulfur oxides. Hence, it is necessary to remove this dye from wastewater (Behera et al. 2017; Ghaedi et al. 2014; Kumar et al. 2014; Rehman et al. 2013; Kumar et al. 2012; Zhang et al. 2011; Nandi et al. 2009).

There are numerous techniques for dye removal, including membrane filtration, coagulation, enhanced oxidation, integrated treatment processes, and adsorption (Akl et al. 2023a, 2023b, 2021; Al-Awadhi et al. 2023; Akl et al. 2022a, b; Serage et al. 2022; Mostafa et al. 2021; Qian et al. 2013; Aziz et al. 2012; Kurt et al. 2012; Lotito et al. 2012; Javaid

et al. 2011). For various applications, including wastewater treatment, purification and liquid mixture separation, or polar organic solute recovery from biotechnology operations, the adsorption process is one of the most straightforward and efficient procedures with simple operating conditions (Akl et al. 2023c, 2022b; Abdel-Fadeel et al. 2022; Rehman et al. 2012).

Using activated carbons as an adsorbent is very common as they have a lot of advantages like they have high capability and efficiency to remove many pollutants, low cost, and simplicity of design. However, the large-scale usage of AC is controlled when it is produced from expensive and nonrenewable precursors despite it being commercially available (Islam et al. 2017; Cherifi et al. 2009; Tan et al. 2008). This has prompted researchers to seek and evaluate other sources for producing AC in feasible ways. Agricultural wastes such as sawdust, banana core, fruit stones, and coconut husks are feasible and promising precursors for activated carbon due to their low cost, availability, and eco-friendly. (Murmu et al. 2019) It is very essential to produce highly efficient activated carbon from low-cost, available, and renewable precursors like biomass-based agroindustrial byproducts (Húmpola et al. 2016; Ioannidou and Zabaniotou 2007). Impressively, different agricultural biomasses have been utilized such as sugar cane bagasse, rice husk and straw, fruit peel, animal waste, date and rape seed, and corncob in order to produce a large amount of biochar (Hai et al. 2019; Idrees et al. 2018; Lam et al. 2018; Meng et al. 2018; Alvarez et al. 2014).

Date palm is one of the oldest plants grown by humans and has been used as food for about six thousand years. It is widely planted in dehydrated and semi-dry areas around the world. Huge numbers of date palm trees are present in Yemen and present in great quantities in Iraq, Saudi Arabia, the United Arab Emirates, Egypt, and the rest of the Arab world. Its scientific name is *Phoenix dactylifera* L. (Mahdi et al. 2018, 2017; Shi et al. 2014). Date fruit output has grown globally, from 4.6 million tonnes in 1994 to 7.68 million tons in 2010, and it is anticipated that this trend will continue (Al-Farsi et al. 2007; Sahari et al. 2007; Besbes et al. 2005). In addition to their nutritional significance, date fruits are believed to have many medicinal activities such as free radical scavenging activities, antioxidant, anti-inflammatory, gastroprotective, hepatoprotective, and nephroprotective activities.

The byproducts of date processing industries include date seeds (date pits). Every year, a lot of dates pits might be produced. Relying upon the date cultivar, the weight (%) of pits varies from 4.6 to 15% of the entire fruit weight (Tang et al. 2013; Ashraf and Hamidi-Esfahani 2011; Al-Bowait. 2006). In the future, the Arab World will have access to over 100,000 tons of date pits each year, which are currently being wasted. It is a difficulty when it comes to collection, no doubt. The modern food processing sector, which exports dates with the pits removed, would be the best source for their collection and successful use.

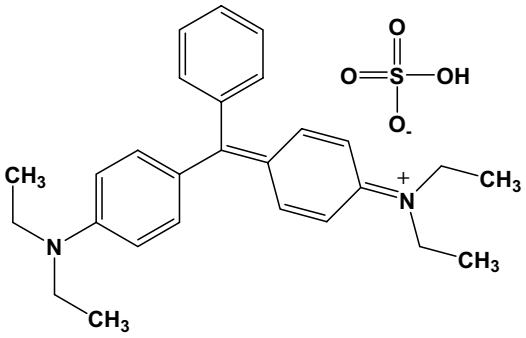

Scheme 1 The structure of Brilliant Green dye ($C_{27}H_{34}N_2O_4S$)

Even though activated carbon is a significant commercial product on the chemical market, production of it in our nation has not yet begun. This stimulated the authors to prepare date pit activated carbons, describe them and investigate their adsorption capabilities for dyes and heavy metals.

The present study was carried out with the following objectives:

(i) Design and characterization of from zinc chloride activated carbons from date pits (ZCPs) using various instrumental performances as Fourier transform infrared spectroscopy (FTIR) and scanning electron microscopy (SEM).
(ii) Batch sorption experiments utilizing cationic dye (BG) as pollutant.
(iii) Studying the optimum conditions of the BG adsorption such as the BG initial concentration, ZCPs weights, pH, temperature, isotherms, kinetics, thermodynamics, and shaking time.
(iv) Comparative evaluation of removal efficiency of BG dye, feasibility, and reusability of with other adsorbents.
(v) Elucidation of the mechanisms involved in the processes of activation of date pits derived carbons using zinc chloride.
(vi) Elucidation of the mechanisms involved in the processes of adsorption of BG onto zinc chloride activated carbons from date pits (ZCPs) composite.

Experimental

Materials

Date pits were bought from market, in Marib City, Yemen. Brilliant Green Dye ($C_{27}H_{34}N_2O_4S$) that present in Scheme 1, was used as it is without any purifications and

was purchased from Merck Company (Germany) (Almana and Mahmoud 1994). In order to prepare BG 1000 ppm, 1 g of the BG was dissolved in a liter of distilled water. The concentration of the other solutions tested in the current study can be changed by the diluting method. The pH adjustment for the BG solutions occurred by utilizing NaOH and HCl (diluted solutions) (Almana and Mahmoud 1994).

Preparation of date pits derived -Zinc Chloride-activated carbon (ZCPs)

Date pits were powdered, pretreated by washing with 0.5% HCl to remove all dirt, dried in an oven at 378K overnight, ground by a mill, sieved to mesh size of 1–4 mm, and carbonized in a tabular furnace at 873K for 2h to yield the carbonized samples (CPs). CPs was rinsed for one day in Zinc chloride ($ZnCl_2$) solution with an impregnation ratio of $ZnCl_2$: char (w/w) equal to 1:1(ZCP11), 2:1(ZCP21) and 3:1(ZCP31). The mixture was then dried in an oven all-night at 378K to remove moisture and followed by the activation step at 1023 K for 2h. The resulting ZCPs were washed with dist.H_2O many times after cooling until the pH of the filtrate reached 7. This was followed by drying the ZCPs overnight in an oven at 378K. The activated carbons were then repeatedly rinsed in hot dist.H_2O to remove any excess chloride ions (Tang et al. 2019; Almana and Mahmoud 1994).

Characterization

Through using a surface Area and Size Analyzer (QUANTACHROME–NOVA 2000 Series) and by applying Brunauer–Emmett–and–Teller (BET) equation and N_2 adsorption–desorption measurements, the ZPCs biosorbents surface area was obtained at liquid nitrogen temperature, 77 K. The surface micrographs of the biosorbents (ZPCs) were captured utilizing a JSE–T20 (JEOL, Japan) scanning electron microscopy (SEM) apparatus at 40 kW. The samples were totally dried at 383 K prior to analysis, and a thin coating of Au particles was applied to them in order to dissipate sample metallization and charges. The FTIR spectra of the prepared activated carbons before and after activation with $ZnCl_2$ and after the BG adsorption using a Nicolet FTIR spectrophotometer instrument in the range of 4000 to 400 cm^{-1}. The samples were prepared by mixing 1 mg of each sample with KBr (500 mg). The scanning occurred in the 4000 to 400 cm^{-1} range. The type of carbon surface and the amount of the functional groups that exist on it were estimated via neutralization with bases of differing strengths by applying the acidity of the surface and Boehm titration approaches.

The moisture content is estimated by heating 50 mg of the biosorbent in an oven at 110 °C overnight, then it was cooled in desiccators to 25 °C and finally weighed. To calculate how much ash is in the produced biosorbent by putting 500 mg of the sample in a muffle furnace at 700 °C for six hours. The residual minerals that are present as impurities in the adsorbent are left behind after the carbonaceous component of the adsorbent is burnt off during pyrolysis. According to reported work (Litefti et al. 2019; Nemr 2009), the point of zero charge (pH_{PZC}) for the prepared material was assessed. A pH meter (Hi 931,401, HANNA, Portugal) device was utilized to measure the solution's pH. The batch sorption experiments were carried out at 240 rpm on a Shaking Water Bath (Nickel Electro Ltd., NE5, UK).

Batch adsorption studies

The current investigation utilized the batch approach, 50 ml of known concentration of the BG solution was put in a 250ml glass stoppered bottle with a known dose of ZCPs. At room temperature, the bottles were kept in a thermostatic shaker with a constant speed of 240 rpm. After the equilibrium was reached, the supernatant solution that includes the remains of the investigated BG was measured at its specific λ_{max}. Various parameters were investigated like contact time, temperature (25–45 °C), CP and ZCPs dose (0.025–0.2 g), pH (from 2 to 10), ionic strength, and initial BG concentration of (50–500 mg/l). The BG pollutant removal percentage (R, %) and adsorption capacity (q_e, (mg/g)) were calculated in Eq. (1) and Eq. (2), respectively (Bakr et al. 2018; Qi and Xu 2004). The BG concentration was measured spectrophotometrically at lambda maximum (λ_{max}) 624 nm. The BG pollutant removal percentage (R, (%)) and adsorption capacity (q_e, mg/g) were calculated in Eq. (1) and Eq. (2), respectively (Bakr et al. 2018; Qi and Xu 2004).

$$q_e = \frac{(C_i - C_e)V}{m} \quad (1)$$

$$R\% = \frac{(C_i - C_e)}{C_i} \times 100 \quad (2)$$

where C_i (ppm) and C_e (ppm) are the initial BG concentration and equilibrium BG concentration after adsorption, respectively. V (L), is the volume of BG solution, and *m* is the mass of the ZCPs adsorbent (g).

Adsorption isotherms investigations

The equilibrium adsorption isotherm investigation is critical in representing the solute and adsorbent interactive behavior and is also important for the design of the adsorption system of BG pollutant adsorption.

Langmuir isotherm

The Langmuir model, Eq. 3, illustrates the monolayer adsorbate adsorption onto a homogeneous adsorbent surface. Also, the maximum capacity can be estimated by it (Mittal et al. 2015; Goscianska et al. 2014).

$$\frac{C_e}{q_e} = \frac{1}{bq_m} + \frac{C_e}{q_m} \tag{3}$$

As q_e and q_m, which are expressed by mg/g, are the quantity of the BG at equilibrium and the maximum adsorption capacity, respectively, while b (L/mg) is the Langmuir constant.

A separation factor, R_L, is performed to investigate the Langmuir isotherm and is calculated as in Eq. 4.

$$R_l = \frac{1}{1 + K_l C_o} \tag{4}$$

The highest initial concentration of the solute is C_o. The separation factor, R_L, reveals the isotherm type and the adsorption process characteristics. If the R_L equals 0, equals 1, between 0and1, higher than 1 the adsorption can be irreversible, linear, favorable, or unfavorable, respectively (Tang et al. 2019).

Freundlich isotherm

It is often employed for heterogeneous surface energy systems and is described by Eq. 5 (Bakr et al. 2018; Qi and Xu 2004; Almana and Mahmoud 1994).

$$\ln q_e = \ln K_f + \frac{1}{n} \ln C_e \tag{5}$$

where C_e, k_f, and q_e are the equilibrium concentration in the liquid phase (mg/l), Freundlich constant, and the adsorption capacity (mg/g), respectively. n is the empirical parameter depicting the energetic the adsorption sites heterogeneity.

Kinetic studies

The BG adsorption onto the ZCPs surface was described by the following four kinetic models:

Pseudo-first-order

The pseudo-first-order kinetic model is represented by Eq. 6 (Bakr et al. 2018; Qi and Xu 2004; Almana and Mahmoud 1994).

$$\log(q_e - q_t) = \log q_e - \frac{k_1}{2.303} t. \tag{6}$$

whereas q_e and q_t are the amount of BG loaded per mass of the ZCPs biosorbent at equilibrium and at a specific time (t, min), respectively; while k_1 is the rate constant, 1/min.

Pseudo-2nd-Order

This model is represented by Eq. 7 (Bakr et al. 2018; Qi and Xu 2004; Almana and Mahmoud 1994).

$$\frac{t}{q_t} = \frac{1}{k_2 q_e^2} + \frac{t}{q_e} \tag{7}$$

where k_2 is the rate constant.

Weber—Morris intraparticle diffusion

The intraparticle diffusion mechanism was investigated to understand the BG adsorption process's diffusion mechanism by utilizing Weber and Morris equation, Eq. 8 (Bakr et al. 2018; Qi and Xu 2004; Almana and Mahmoud 1994).

$$q_t = k_{int} t^{1/2} + C \tag{8}$$

where the intercept, C, is found by plotting qt against $t^{1/2}$, and k_{int} (g/mg $min^{1/2}$) is the adsorption constant (Mittal et al. 2014).

Boyd's equation

The kinetic data were then assessed utilizing Boyd's delivered kinetic expression to determine whether adsorption happens through an external diffusion or an intraparticle diffusion mechanism which is stated in Eq. 9 (Bakr et al. 2018; Qi and Xu 2004; Almana and Mahmoud 1994).

$$F(t) = 1 - \frac{6}{\pi^2} \sum_{n=1}^{\infty} \frac{1}{n^2} \exp\left(-n^2 Bt\right) \tag{9}$$

where B (t) is a mathematical function of F. While F is the fraction of equilibrium at various times (t) and n is an integer that determines the infinite series solution and is obtained by the expression, Eq. 10.

$$F = \frac{q_t}{q_e} \tag{10}$$

Equation (9) can be rewritten to:

$$B_t = -0.4977 - \ln(1 - F) \tag{11}$$

Thermodynamic studies

Thermodynamic parameters for the adsorption of BG on the ZCPs biosorbents are evaluated by the equilibrium

experimental data observed at different temperatures from 298.15k to 318.18 K.

The difference in the thermodynamic distribution coefficient, kc, with a temperature change was utilized to determine thermodynamic parameters. The following equations were applied to calculate the standard free energy change, ΔG°, Eqs. 12 and 13.

$$\Delta G^{\circ} = -RT\,ln\,k_C \tag{12}$$

$$\Delta G^{\circ} = \Delta H^{\circ} - T\Delta S^{\circ} \tag{13}$$

As Kc, T, and R are the Langmuir constant, the absolute temperature in K, and the gas constant (8.314 J/(mol. K)), respectively. The entropy (ΔS°) and standard enthalpy (ΔH°) of adsorption may be computed utilizing the Van't Hoff equation, Eq. 14:

$$\ln k_C = \frac{\Delta S}{R} - \frac{\Delta H}{RT} \tag{14}$$

where K is the equilibrium constant (g^{-1}). By plotting the graph between 1/T and ln(k), the adsorption process ΔH° and ΔS° were estimated from the slope and the intercept (Bakr et al. 2018; Qi and Xu 2004; Almana and Mahmoud 1994).

Desorption experiments

Desorption investigations were carried out after the adsorption process by utilizing various eluent agents: absolute EtOH, HNO_3, HCl, NaOH, and $NaHCO_3$ with concentrations (0.01–0.5 M). Briefly, 0.2 g of BG-loaded ZCPs was immersed in 10 mL of eluent solution for 3 days with shaking at 150 rpm. Then the desorbed BG concentration was analyzed spectrophotometrically after the suspension was stirred for a fixed time. The BG desorption efficiency can be estimated using equation, Eq. 15 (Bakr et al. 2018; Qi and Xu 2004).

$$\text{Desorption}\% = \frac{\text{Desorbed amount of BG}}{\text{Total Adsorbed amount of BG}} \times 100\% \tag{15}$$

Results and discussion

Materials' design and physicochemical studies

Analysis of the carbons' nitrogen adsorption–desorption data

Both carbons porosity and surface area play effective roles in adsorption capacities (q_e) improvement (Brunauer et al. 1938). Conventionally, the adsorption of nitrogen at 77 k is used to measure the textural proprieties of solids, and adsorption data are commonly analyzed utilizing the BET equation (Akl et al. 2013).

The N_2 adsorption/desorption isotherms of ZCP11 and ZCP31 carbon samples are represented in (Fig. 1a). It displays shapes that are similar to one another. The Types IV and V isotherms, which are typical of mesoporous materials, are indicated by these shapes, according to the IUPAC classification. (Fig. 1b) displays the linear BET plots for all sorbents of nitrogen adsorption at 77K.

BET

The surface area, S_{BET}, values of the ZCPs materials can be determined by utilizing the linear BET plots of N_2 adsorption at a temperature of 77 K, which show varied surface area values relying on modification and activation processes. The specific surface areas of CP, ZCP11, ZCP21, and ZCP31 were found to be 165.91, 289.51, 333.84 and 667.89 m^2/g, respectively, as shown in Table 1. The ZCPs' S_{BET} values can offer various active sites that result in an increase the BG adsorption. $ZnCl_2$ activation process is characterized by the formation of both wide microspores and small mesopores where $ZnCl_2$ acts as dehydrating agent. The degradation and dehydration of cellulosic material caused by the impregnation of the precursor with $ZnCl_2$ lead to carbonization, aromatization of carbon skeleton and pore structure formation. Pore formation can be attributed to releasing of hydrogen gas during the decomposition of phenolic-aromatic structure of the precursor resulting in formation of porous structure and active sites (Youssef et al. 1994). The volume of pores developed is similar to the volume of $ZnCl_2$ introduced into the particles; so, increasing the $ZnCl_2$ impregnation ratio results in increasing in S_{BET} values which increase from 289.51 m^2/g for ZCP11to to 667.89 m^2/g for ZCP31.

Activation mechanism Chemical activation agents such as $ZnCl_2$ are frequently employed (Chang et al. 2013; Sun et al. 2013; Yue and Mangun 2002; Hu et al. 2001). Even though a distinct process of chemical activation is employed to produce carbons with numerous porous, the approach is not completely understood. In the beginning, a temperature over 500 °C is suitable for the activation step because the $ZnCl_2$ melting point is 283–293 °C. Meanwhile, the Zn^{2+} radius of 74 Pico meters is less than that of common metal salt ions such as Na^+ (102 Pico meter), K^+ (138 Pico meter), and Ca^{2+} (100 Pico meter), which can contribute to the ZCPs to obtain micropores from 0.54 to 1.311 nm. $ZnCl_2$ is additionally typically thought of as a dehydrator (Sun et al. 2013; Hu et al. 2001). On the one hand, at high concentrations of zinc chloride, $ZnCl_2$ combines with H_2O to create hydroxy dichloro zinc acid ($ZnCl_2 + H_2O \rightarrow H\,[ZnCl_2(OH)]$). To clean the

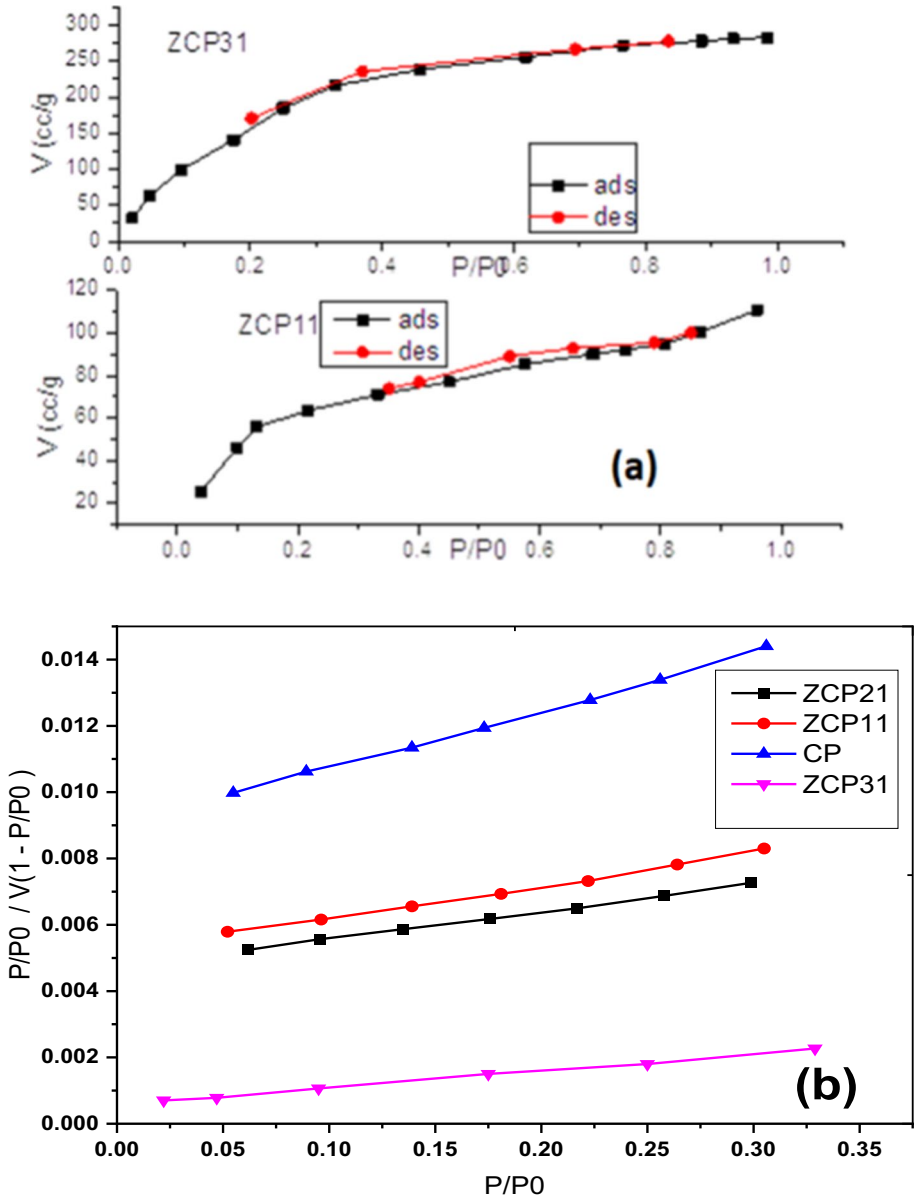

Fig. 1 **a** Nitrogen adsorption-desorption isotherms at 77K for ZCP11, and ZCP31; **b** nitrogen adsorption linear BET plots at 77K for CP, ZCP11, ZCP21 and ZCP31

Table 1 The textural properties of ZCPs

Sorbent	S_{BET} (m^2/g)	BET/C constant	V_T (cm^3/g)	Aver. pore r (nm)
CP	165.91	2.92	0.047	0.54
ZCP11	289.51	2.89	0.082	0.565
ZCP21	333.84	2.76	0.091	0.544
ZCP31	667.89	21.18	0.438	1.311

CPs impurities and also to make a channel structure, acid that has an etching influence is used. On the other hand, if $ZnCl_2$ is combined with CPs, the amount of $ZnCl_2$ or ZnO ($ZnCl_2 + OH^- \rightarrow ZnO + HCl$) that remains in the pore structure may prevent $ZnCl_2$ from volatilizing as the temperature rises, altering the carbon's pyrolysis behavior and resulting in reduced char (Mittal et al. 2015). At the same time, the carbon yield (%) is found to be higher as a $ZnCl_2$ consequence inducing plenty of H and O atoms in the carbon precursor to be removed as H_2O rather than developing in hydrocarbons or oxygenated organic matter (Jia et al. 2002).

Moisture% and ash content

The produced activated carbon's effectiveness is gauged by its moisture and ash contents. As can be shown in Table 2, the CP (precursor of ZCPs) has a very low moisture and ash content, demonstrating its great activation efficiency.

Table 2 Physicochemical characters of the biosorbents

Type of carbon	Carboxylic (mmol/g)	Lactonic (mmol/g)	Phenolic (mmol/g)	Total Acidic groups (mmol/g)	Basic groups (mmol/g)	Moisture content %	Ash Content %	pH of supernatant Solution	pH_{PZC}
CP	0.163	0.427	0.194	0.784	0.093	4.78	3.66	6.75	6.23
ZCP11	0.204	0.432	0.216	0.925	0.069	8.24	15.11	4.98	5.47
ZCP21	0.214	0.442	0.224	0.959	0.065	8.64	14.82	4.86	5.59
ZCP31	0.261	0.481	0.245	0.987	0.057	9.65	12.27	4.59	5.73

Surface acidity, pH_{PZC} and Boehm titration

The pH of the carbon substance aqueous solution supplies a suitable indicator of the chemical parameters type and concentration for the investigated ACs.

As presented in Table 2, it can be revealed that: -

(i) The pH of the non-active carbon (CPs) surface is neutral, 6.23.
(ii) The pH of surface of ZCPs activated carbons are 4.98, 4.86, and 4.59 for ZCP11, ZCP21, and ZCP31, respectively. This suggests that the surfaces have a modest predominance of acidic functional groups.

The pHpzc, the point of zero charges, is the value of pH at which the totality of positives and negatives charges equals zero on the investigated substance's surface (Jia et al. 2002). At a pH < the carbon pH_{PZC}, its surface is positively charged while it is negative at a pH > the carbon pH_{PZC}. The pH_{PZC} of ZCP11, ZCP21, and ZCP31 is 5.47, 5.59, and 5.73, respectively, as presented in Table 2.

Boehm technique depends on the selective neutralization of the functional groups on the surface in accordance with their acidity because it is known that a functional group with a particular pKa may only be neutralized by a base with a greater value of pKa (Boehm 1994). Bases like sodium hydroxide, NaOH (pKa = 15.74), sodium carbonate, Na_2CO_3 (pKa = 10.25), sodium bicarbonate, $NaHCO_3$ (pKa = 6.37), and sodium ethoxide, $NaOC_2H_5$ (pKa = 20.58) are utilized. $NaHCO_3$ neutralizes carboxylic groups, whereas lactones were neutralized by Na_2CO_3 but not by $NaHCO_3$. Phenols were neutralized by NaOH but not by Na_2CO_3. The neutralization of the surface with NaOH revealed all of the acidic functional groups, including carbonyl groups. The basic groups on the surface of the activated carbon, on the other hand, were detected using HCl.

Table 2 depicts the CP and ZCPs biosorbents' surface acidity and the various acidic groups' existence. An investigation of the data in Table 2 reveals:

(i) The overall surface area of acidic sites is greater than that of basic sites, confirming the acidic character of their surfaces. This observation was completely agreeing with the findings of pH_{SUP}, a pH_{PZC} that is also acidic.
(ii) For $ZnCl_2$ activated carbon samples, the total acidity increases with increasing the impregnation ratios of $ZnCl_2$;
(iii) Lactones > > carboxylic > phenolic is the order of the acidic groups on the surface of all samples.

Characterization

Scanning electron microscopy (SEM)

The SEM images of ZCP11, ZCP21, and ZCP31 are depicted in Fig. 2(a–c), respectively. According to the SEM images, preliminary treatments that included impregnation, crushing, carbonization, and activation at varied temperatures may be to blame for the activated carbons' uneven form, size, and lack of a clearly defined morphology. Due to the effect of various $ZnCl_2$ activating agent ratios, pore development is observed in activated carbon samples. The SEM micrographs, which were taken at magnifications of 1500 × and 3500 x, are quite obvious in revealing the porous structure of the ZCPs.

FTIR spectra

FTIR is an analytical technique used to identify the surface functionalities in activated carbons. Figure 3 shows FTIR spectra of CP, ZCP31and BG-ZCP31 samples.

In the FTIR of CP and ZCP31**,** Figure A and B, before BG adsorption, the carbon samples exhibit a wide band at around (3265–3445 cm^{-1}) wavelength due to the hexagonal group's O–H stretching mode and adsorbed H_2O. Additionally, the carbon samples exhibit the shoulders at (2850–2950 cm^{-1}), which are caused by aliphatic (C-H) molecules (Sain and Panthapulakkal 2006; Kennedy et al. 2005). The stretching vibration of the C-H in the methyl group is responsible for a definite band at 1595–1465 cm^{-1} (Sain and Panthapulakkal 2006). The bands that appear in the region of 1253.414–1015 cm^{-1} may be returned to the stretching vibration of ROH and C-O in acids, phenols, ethers, and

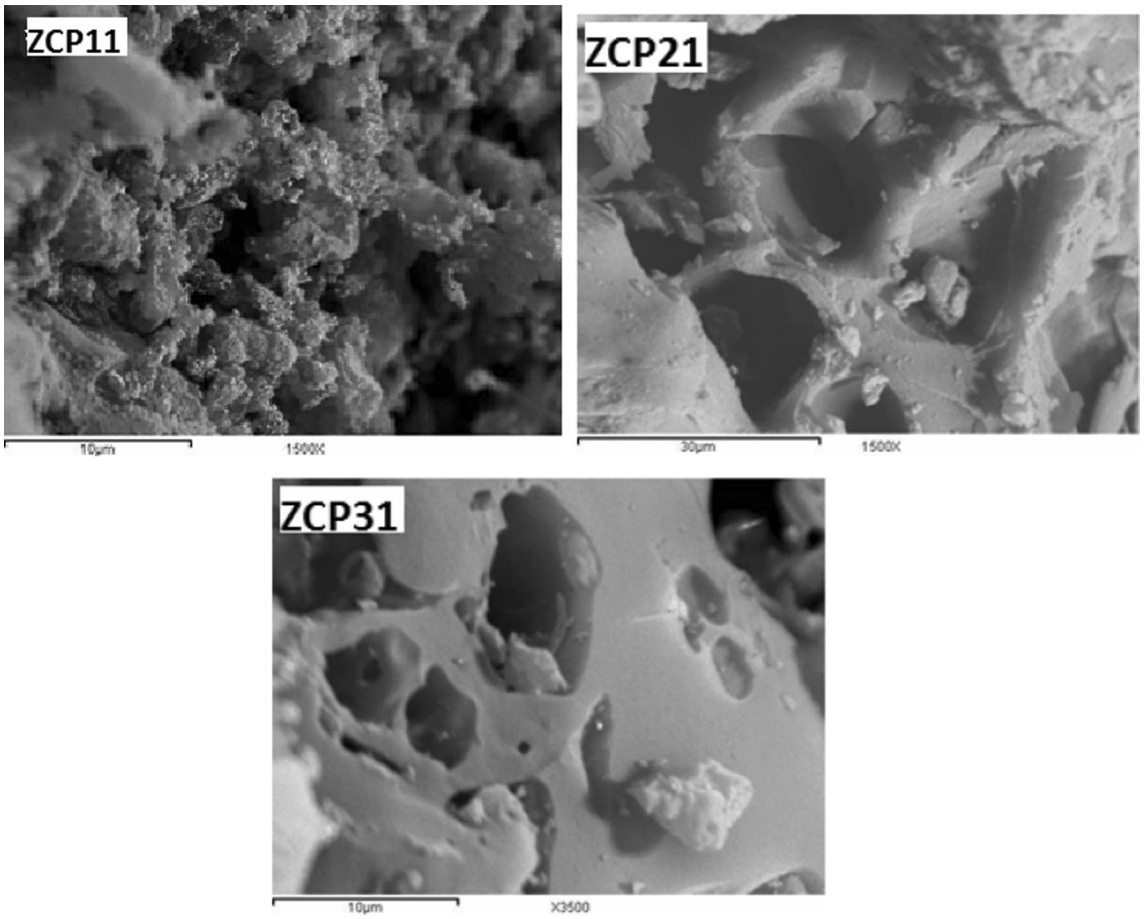

Fig. 2 SEM photographs of **a** ZCP11, **b** ZCP21, and **c** ZCP31

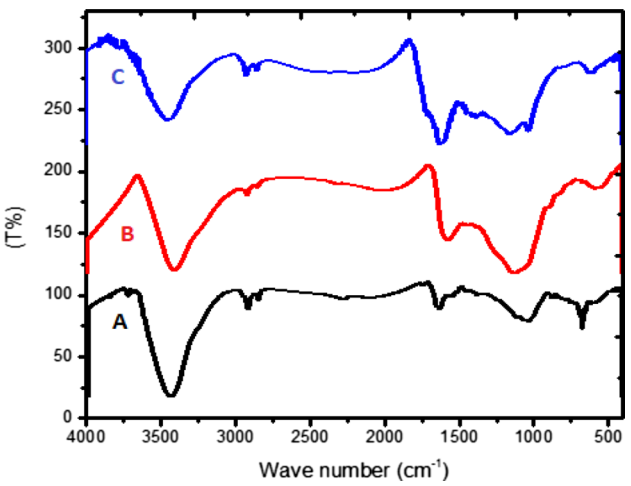

Fig. 3 FTIR spectra of: **a** CP, **b** ZCP31and **c** BG-ZPC31

esters (Southichak et al. 2006). Due to the superposition of several large overlapping bands, it is challenging to assign the bands in the range of 1000–1200 cm^{-1}. This overlapping band has been attributed by some writers to the ether (symmetrical stretching vibrations), phenolic structures and epi-oxide that exist in various structural settings (Kennedy et al. 2004; Gómez-Serrano et al. 1994; Faix 1992). As present in (Fig. 3C), the ZCP31-BG FTIR spectrum was compared with that of CP and ZCP31 showed that there are bands at 3442, 2920, 1583, 1440 cm^{-1}, assigned to O–H, –CH aliphatic, –C=C, $–CH_2$ bending, respectively. Also, showed shifts in bands of the ZCP31-BG FTIR spectrum to higher and/or lower with the appearance or disappearance of other bands, which indicates the complete adsorption of the BG dye.

Adsorption studies

Effect of pH

pH can enormously influence the BG pollutant adsorption in aqueous solutions (Mansour et al. 2020; Jamshidi et al. 2016). The BG pollutant adsorption experiment was obtained over the pH range of 2–10 as shown in Fig. 4. The BG removal [R (%)] gradually increased as the pH increased from 2 to 6, and then it almost remained constant

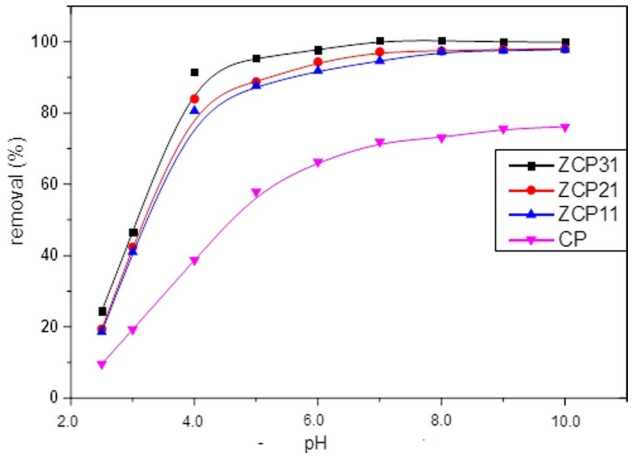

Fig. 4 Effect of The pH on adsorption capacity of BG by CP, ZCP11, ZCP21, and ZCP31. (C_o = 200 mg/l; dose = 0.05 g/50 ml, T = 25 °C)

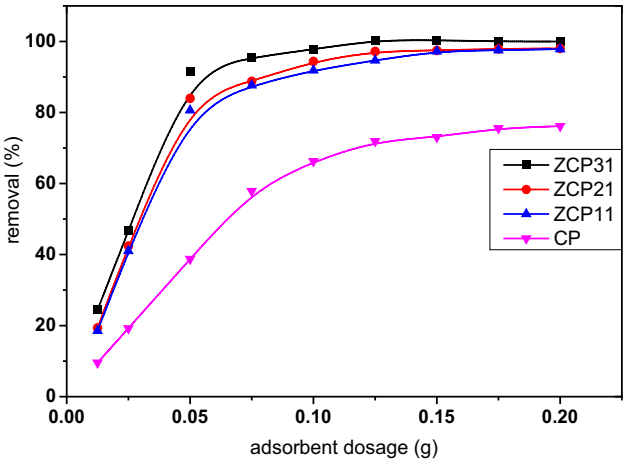

Fig. 5 Effect of the CP, ZCP11, ZCP21, and ZCP31 dosage on the adsorption capacity of BG. (C_o = 200 mg/l; T = 25 °C)

at pH from 7 to 10. The BG-loaded percentage on ZCPs is low in a very acidic pH medium (Fig. 4). The explanation is that, at low pH, protons (H^+) dominate the competitive adsorption process on ZCPs. As illustrated in Table 2, the ZCPs pH_{PZC} is 5.73. The ZCPs surface is negatively charged at a pH higher than its pH_{PZC} which leads to promoting the adsorption of the BG. The pH at which material surface net charges equals 0 is called the pH_{PZC} (Omrani and Nezamzadeh-Ejhieh 2020). The ZCP surface becomes positively charged and prohibits BG pollutant adsorption when the pH is lower than the ZCP pH_{PZC}. As at a pH higher than the pH_{pzc}, the net positive charges decreased which result in a decrease in the repulsion force between the BG pollutant and the ZCP surface. Subsequent experiments were performed at pH 7.0.

Effect of adsorbent dose

The ZCPs' weight effect on the removal of the BG pollutant is represented in Fig. 5. It was noticed that the BG uptake increased as ZCPs' weights were increased. When the ZCPs doses increased from 0.025 to 0.2 g, the removal efficiency of the BG increased significantly from 9.49 to 76.13%, from 18.61 to 97.82%, 19.42 to 98.14% and from 25.03 to 99.97% for CP, ZCP11, ZCP21, and ZCP31, respectively. With the ZCPs' doses increasing from 0.025g to 0.05g, a rapid increase in BG elimination was observed. While increasing the ZCPs doses over 0.1g, the BG removal efficiency not significantly changed. Thus, a 0.05g dose of the ZCPs can be chosen as the optimum dose. The observed BG removal efficiency increase with the ZCPs doses increases may be returned to the surface area and available active sites increase.

Effect of initial BG concentration

The initial BG concentration's influence on the CP and ZCPs material adsorbing capacity to the studied pollutant (BG) was examined, as displayed in Fig. 6. Once the dye concentration was raised, it was determined that the CP and ZCPs' capacity to adsorb the BG increased as well. As the concentration increased from 50 to 500 mg/l, the sorption capacity, q_e, increased from 42.092 to 75.28 mg/g for CP, from 46.067 to 200.185 mg/g for ZCP11, from 47.57 to 210.11 mg/g for ZCP21, and from 49.719 to 247.75 mg/g for ZCP31. This may be caused by the rise in the adsorbate's concentration as an impetus to overcome the BG's mass transfer barrier between the solid and liquid phases. However, it should be noticed that as the initial BG concentration (C_o) increased from 50 to 500mg/l, the R (%) was lowered, in spite of the

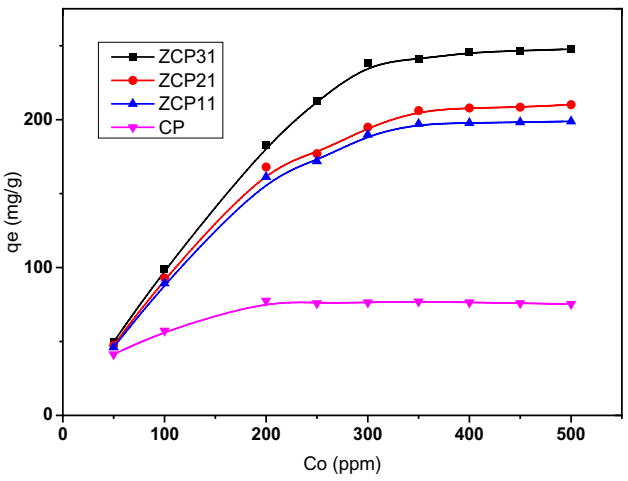

Fig. 6 Effect of The the initial dye concentration on adsorption capacity of BG by ZCPs. (dose = 0.05 g/50 ml, T = 25 °C)

carbons uptake capability (q_e) increased. The active sites' saturation with an increase in the initial concentration of BG may be the reason for the dye removal (%) decrease at $C_o = 500$ mg/l.

Adsorption isotherms

The adsorption isothermal study is applied to relate the adsorbed BG amount at the interface and the adsorbent (ZCPs) concentration in the bulk solution. These investigations are very important for the design of BG adsorption onto the ZCPs mechanism. The R^2, correlation coefficient, is utilized to detect the most fitting isotherm model to aid in the description of the BG adsorption process.

Langmuir isotherm

Experimental data may be linearized using the linear form as seen in Fig. 7 by plotting C_e/q_e against C_e. For CP, ZCP11, ZCP21, and ZCP31, respectively, the q_m (mg/g), which measures the highest adsorption capacity of ZCPs, is found to be 74.98, 192.02, 201.02, and 247.75. Furthermore, all values of the separation factor (R_L) in the present study ranged between 0.003 and 0.012 confirming that all adsorbents exhibit favorable BG adsorption.

Freundlich isotherm

Figure 8 illustrates the linearized Freundlich model for the BG adsorption onto the ZCPs materials.

Table 3 represents the experimental results of the isotherm parameters. R^2 of both Langmuir and Freundlich models for ZCPs are 0.999 and 0.969, respectively. Langmuir is well fitted to BG adsorption data which suggests that the BG adsorption into ZCPs is a monolayer process.

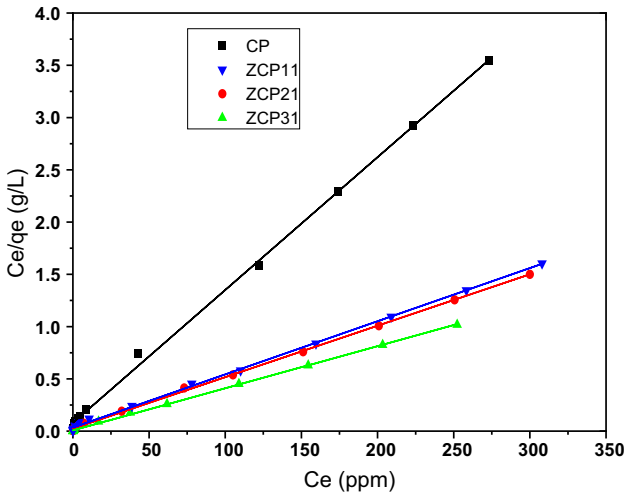

Fig. 7 Langmuir model for brilliant green dye onto ZCPs

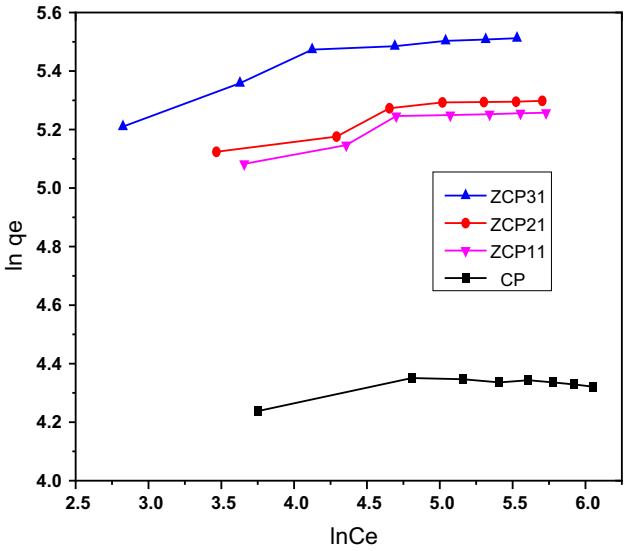

Fig. 8 Freundlich model for brilliant green dye onto ZCPs

Adsorption kinetics

Kinetic investigations provide essential information that assists in the explanation of the BG dye and the ZCPs interaction mechanism. In order to determine the equilibrium time (qt) for BG adsorption by the ZCPs, the shaking time effect was investigated. As shown in Fig. 9 all kinetic curves for BG adsorption by the ZCPs biosorbents are very similar and formed of rapid initial adsorption followed by very slow diffusion. This may be attributed to the availability of a higher surface area at the beginning. Thus 80% of the adsorption was obtained in the first hour while the adsorption reaches its equilibrium after 2 h.

Various models were utilized to investigate the behavior of the BG adsorption on the ZCPs as presented in Table 4 and Fig. 10(a–b) like Boyed, intraparticle diffusion, the

Table 3 Parameters of Freundlich and Langmuir isotherm for BG adsorption by CP, ZCP11, ZCP21and ZCP31

Adsorbents		CP	ZCP11	ZCP21	ZCP31
Langmuir	q_{exp} (mg/g)	74.98	192.02	201.02	247.75
	q_{max}, fitted	79.078	197.46	203.25	248.139
	b (L/mg)	0.1597	0.1534	0.214	0.594
	R_L	0.012	0.013	0.010	0.003
	R^2	0.999	0.9987	0.9993	0.9996
Freundlich	K	75.055	120.10	129.04	143.015
	1/n	0.0084	0.312	0.0819	0.10802
	R^2	0.969	0.802	0.8703	0.83912

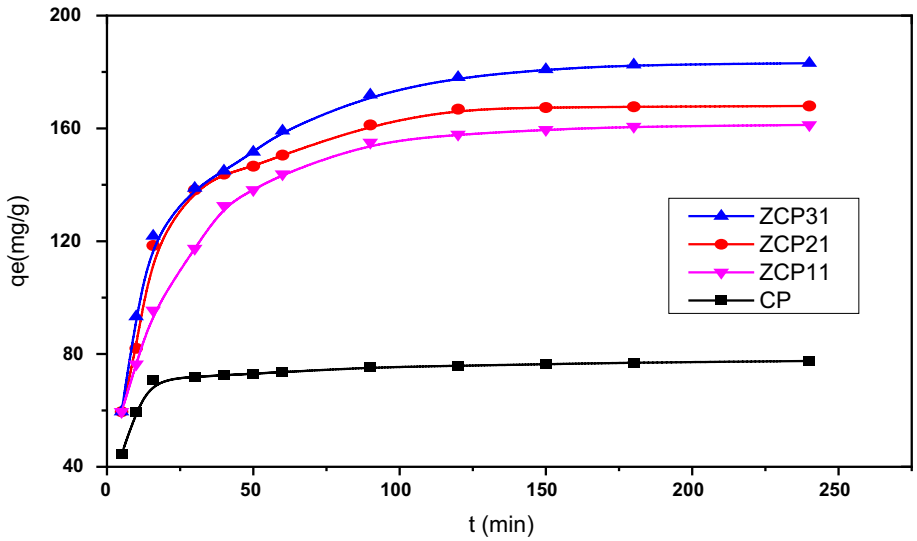

Fig. 9 Effect of contact time on adsorption capacity of BG by ZCPs. (C_o = 200 mg/l; dose = 0.05 g/50 ml, T = 25 °C)

Table 4 Kinetic parameters for the BG adsorption adsorption

Adsorbents		CP	ZCP11	ZCP21	ZCP31
	qe,exp(mg/g)	78.028	127.02	172.15	192.14
First-order kinetic equation	q_1 (mg/g)	16.556	111.05	109.02	131.085
	k_1 (min^{-1})	0.0231	0.0310	0.0373	0.0271
	R_1^2	0.7734	0.9954	0.9542	0.988
Second-order kinetic equation	q_2 (mg/g)	79.17	172.04	177.15	196.29
	k_2 [g/(mg min)] × 10^{-6}	6.94	2.39	1.652	1.94
	R_2^2	0.9999	0.9993	0.9996	0.9988
Intraparticle diffusion equation	k_{int} [mg/(g $min^{1/2}$)]	0.7459	7.9081	5.6331	8.5324
	C	68.0158	83.14275	107.859	92.304
	R_{int}^2	0.99706	0.9986	0.98856	0.9894
Boyd equation	Intercept	1.1803	− 0.0692	− 0.01191	− 0.251
	R^2	0.8698	0.996	0.983	0.9884

pseudo-first-order, and pseudo-second-order models. According to the values of the R2, the pseudo-second-order model matches better than the pseudo-first-order model which indicates the BG adsorption onto the ZCPs is chemisorption. By applying the intraparticle diffusion kinetic model it was proved that there are three main steps implicated in the BG adsorption onto ZCPs biosorbents. The first step is the most rapid and explained as follows BG particles diffused to the ZCPs surface. The second linear stage is an intraparticle BG diffusion inside the ZCPs pores. The third, slow, and final step is a diffusion of the BG particles into the inner micropores of the biosorbents. Furthermore, as it can be noticed from Fig. 10(c–d) none of the straight lines in the intraparticle diffusion and Boyed models passed through the origin indicating that there are other limiting factors that participate in the adsorption process in addition to intraparticle diffusion.

Effect of temperature

The effects of temperature on adsorption were investigated at 298, 308 and 318 k. The results are displayed in Table 5. As it can be noticed, the maximum amounts of BG adsorbed by CP, ZCP11, ZCP21, and ZCP31 carbons are found to have raised when the temperature was changed from 298 to 318 k, from 75.280 to 89.292 mg/g, from 192.022 to 208.103 mg/g, from 210.11 to 218.878 mg/g, and from 247.75 to 254.161 mg/g for CP, ZCP11, ZCP21 and ZCP31, respectively. The increase in adsorption capacity may be brought about by chemical reactions between adsorbent sites and adsorbate or by the raised rate of BG molecule intraparticle diffusion into the carbon pores at higher temperatures (Tang et al. 2019).

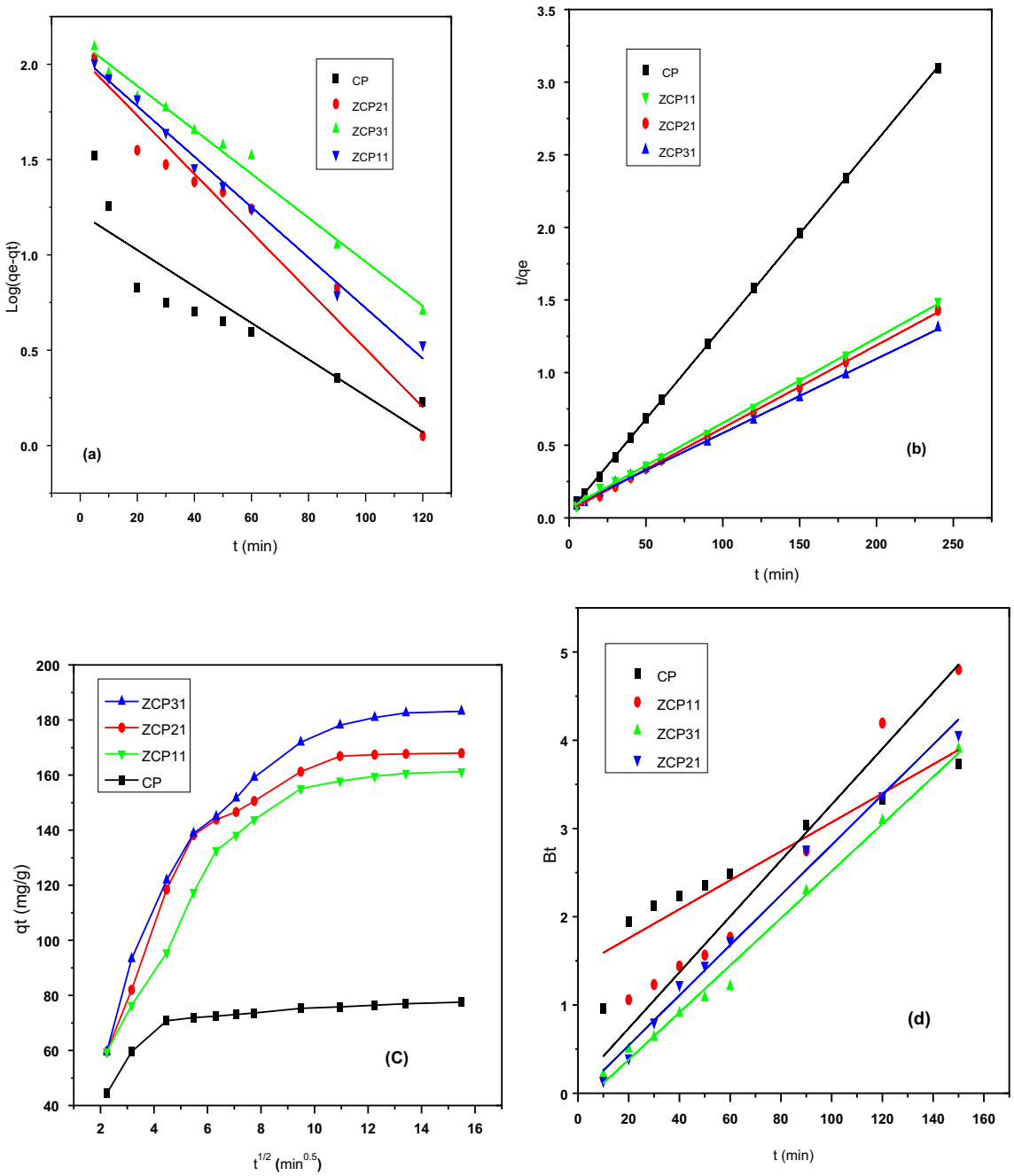

Fig. 10 Kinetic models **a** Pseudo-first-order; **b** Pseudo-second-order; **c** Intraparticle diffusion, and **d** Boyd plot

Table 5 Temperature effect on maximum adsorption capacities of BG by CP, ZCP11, ZCP21and ZCP31

Adsorbent	Q_e (mg/g)		
	298 k	308 k	318 k
CP	75.280	82.023	89.292
ZCP11	200.185	199.83	208.103
ZCP21	210.11	221.24	228.998
ZCP31	247.79	250.719	255.071

Thermodynamic studies

The thermodynamic parameters (ΔG^0, ΔH^0, and ΔS^0) study reveals a lot of information on internal energetic changes and they are calculated as was reported in Sect. "Thermodynamic Studies". As presented in Table 6, it can be detected that with the temperature increasing from 25 to 45°C, the maximum adsorption capacity increased, which specifies an endothermic reaction of the adsorption process for BG on

Table 6 Thermodynamic factors for the BG adsorption by CP, ZCP11, ZCP21, and ZCP31 at various temperatures

Sample code	ΔH° (KJ/mol)	ΔS^0 (KJ/mol K)	ΔG^0 (KJ/mol)		
			298 K	308 K	318 K
CP	66.10	0.30	−22.09	−27.30	−27.75
ZCP11	12.20	0.13	−25.67	−26.60	−28.18
ZCP21	23.05	0.16	−26.39	−27.17	−29.62
ZCP31	46.20	0.25	−28.12	−30.66	−33.16

ZCPs. As shown in Fig. 11, the plot of q_e/C_e vs T^{-1} was linear over the utilized temperature range.

In Table 6, the positive ΔH^0 and negative ΔG^0 values affirm the BG adsorption on the ZCPs to be an endothermic process and spontaneous, respectively. While the positive ΔS^0 value is derived from the enhancive randomness on the solid–liquid interphase. In addition, the increase of the ΔG^0 absolute value with temperature increase illustrates that the rising temperature can increase the adsorption spontaneity.

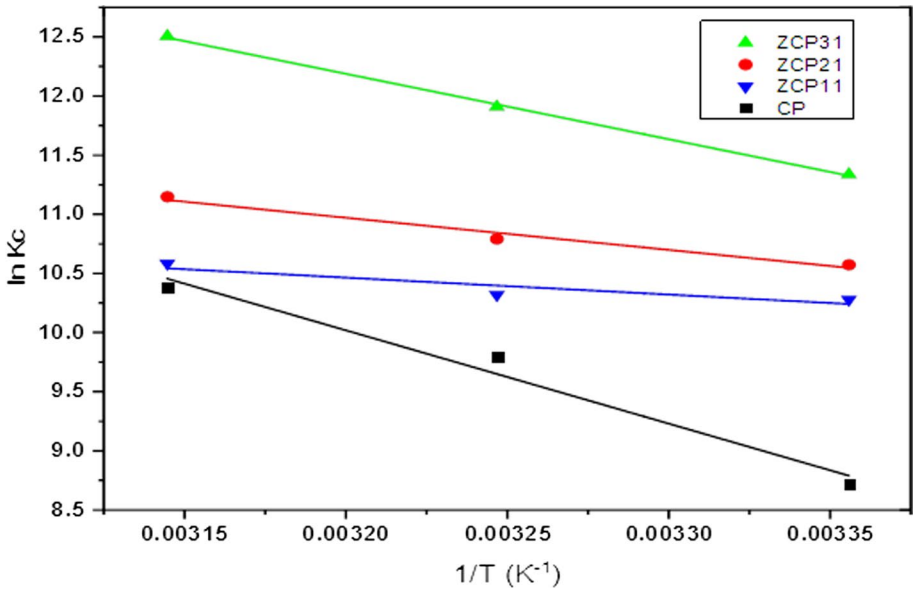

Fig. 11 Thermodynamic parameters ($\ln K_c$ vs 1/T) for the adsorption of BG dye onto ZCPs

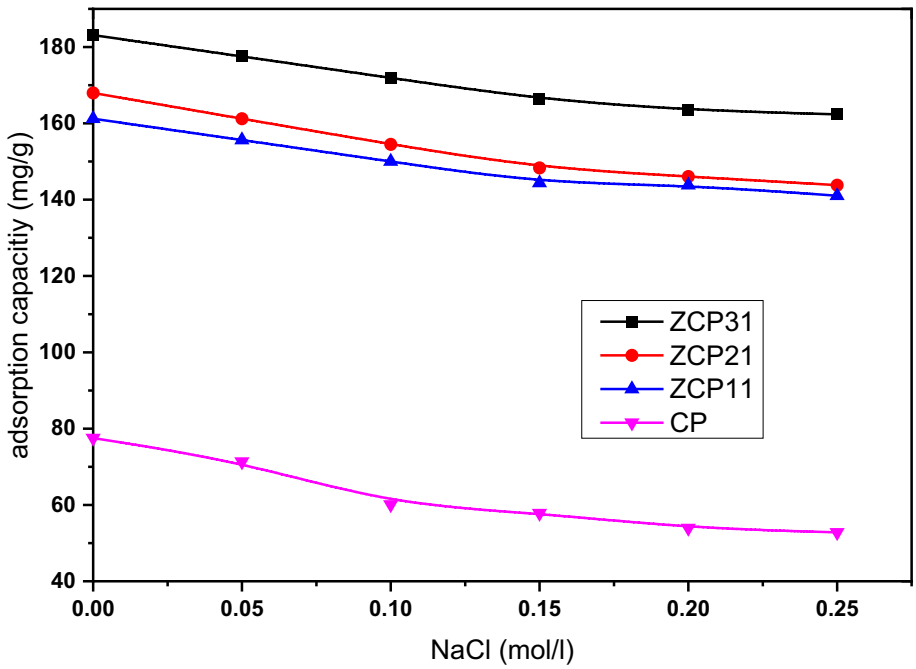

Fig. 12 Effect of Ionic strength effect on adsorption capacity of BG by CP, ZCP11, ZCP21, and ZCP31. (C_o = 200 mg/l; dose = 0.05 g/50 ml, T = 25 °C)

Effect of ionic strength

The influence of ionic strength on the adsorption of BG is shown in Fig. 12. It was shown that when ionic strength increased, the adsorption capacity decreased. The adsorption capabilities for CP, ZCP11, ZCP21, and ZCP31 fell from 77.628 to 52.799 mg/g, from 162.015 to 141.20 mg/g, from 168.021 to 144.131 mg/g, and from 183.419 to 162.417 mg/g, respectively, when the concentration of NaCl increased from 0.05 to 0.5 M. The BG and cations may have been competing with one another for the active sites on the adsorbent surface, which could account for this.

Desorption and reusability studies

Desorption of BG from the BG loaded ZCPs was carried out using 0.2 and 0.4 M HCl. The adsorbent was treated with 50 ml of 0.2 or 0.4 M HCl and stirred until equilibrium to remove the adsorbed BG was collected after being loaded with 100 mg/l of BG at the ideal pH. Table 7 shows that the percent recovery of BG for the adsorbents ZCP11, ZCP31, and CP increased with an increase in HCl from 0.2 to 0.4 M and thereafter stayed constant. The percentage of desorption is shown to have increased from 42.11 to 76.835%, from 47.099 to 81.466% and from 54.475 to 93.847% for ZCP11, ZCP31 and CP, respectively.

As presented in Table 8, the reusability study further demonstrated that the sorbent may be utilized again for 5 times with only a little reduction in adsorption capacity.

Plausible mechanism of adsorption of BG onto ZCPs

The BG adsorption on the ZCPs biosorbents might be returned to numerous interactions like pore-filling, electrostatic attraction, π–π, and H-bonding interactions (Cheng et al. 2021a, b). A schematic representation of the probable BG adsorption process onto ZCPs is presented in Figs. 13 and 14. The BG adsorption occurred at pH greater than the pH_{pzc}; hence, the ZCPs surface will gain negative charges that interact with the positive charges on the BG this interaction is called electrostatic forces (Fig. 14a) (Cheng et al. 2021a, b). Also, the molecules of the BG can be entered into the ZCPs structure through their micropores and mesopores, and thus, they will subsequently adsorb onto the active sites this process is called pore-filling. The nitrogen atoms of the brilliant green interacted with the hydrogen of the ZCPs' OH groups in order to form the hydrogen bond (Fig. 14b) (Cheng et al. 2021a, 2021b). π–π interactions (Fig. 14c) occurred through BG's aromatic backbone interacting with the ZCPs hexagonal skeleton (Cheng et al. 2021a, b).

Table 8 Repeated adsorption cycles of BG by ZCP31 dose (0.025 g), time of shaking 400 min

Cycle number	1	2	3	4	5
Recovery (%)	91.63	91.33	90.54	89.77	89.0

Analytical applications

Analysis of real water samples

Bidistilled water and tap water samples were collected from our lab (Saba Region University, Marib, Yemen), Wastewater was collected from sewage drainage station-Ibb, Yemen and underground water was collected from Ibb city, Yemen. A sintered glass G4 filter was used to filter all of the samples. All of the selected samples were then preserved in plastic containers for later use after being acidified with strong nitric acid to pH 2. The organic matter was digested using $K_2S_2O_8$ (0.5–1.0g) which was added to 1L of the chosen water sample and then the mixture was heated for 30 min at 95 °C. After cooling to 25 °C, 80 mg of ZCPs biosorbents were added to a series of transparent stoppered bottles containing different concentrations of BG (0.0, 5, and 10 ppm) at optimum pH and They were shaken at 150 rpm on a shaker for 4 h and then filtered. Another dose of the ZCPs biosorbents (80 mg) was added to the previous filtrate and the pH was adapted to the optimum then the mixture was stirred for 15 min and filtered. The results that are present in Table 9 showed that the prepared ZCPs were successfully applied for the removal of known amounts of BG spiked to different natural water samples. The recovery % ranged between 70.00 and 82.0% for CP and between 90.7 and 98.0 % for the ZCP31 with

Table 7 Desorption of BG from ZCPs using HCl (0.2–0.4M)

		The BG desorption using 0.2 M HCl		The BG desorption using 0.4 M HCl	
Adsorbent	q_e adsorbed (mg/g)	q_d desorbed (mg/g)	Desorption %	q_d desorbed (mg/g)	Desorption%
ZCP11	92.98	39.15	42.11	71.44	76.835
ZCP31	98.88	46.57	47.099	80.55	81.466
CP	89.33	48.66	54.475	83.83	93.847

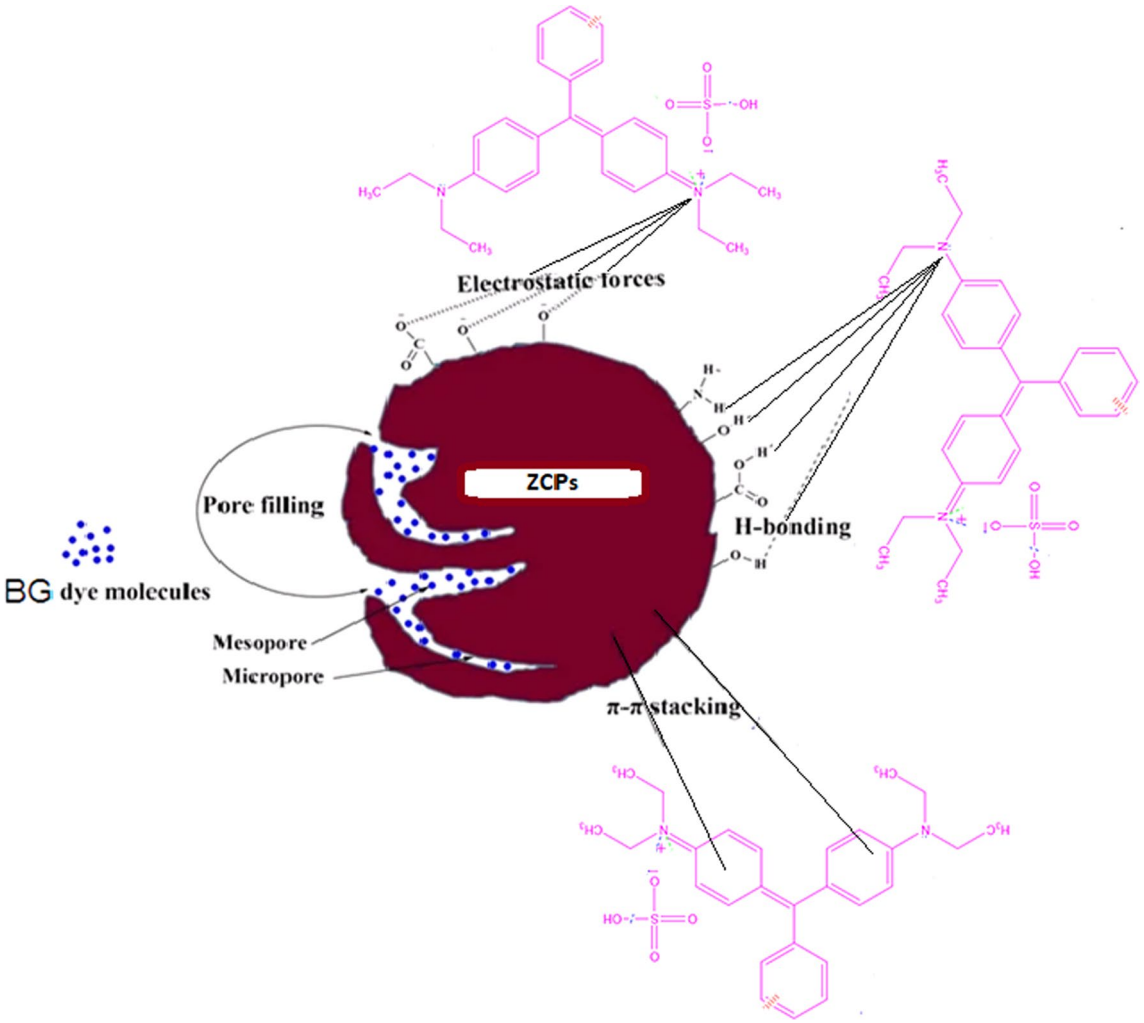

Fig. 13 Schematic illustration of the potential BG adsorption process onto ZCPs

a relative standard deviation lower than 3 (RSD, %, <3). The noticeable increase in the recovery % using ZCP31 can be returned to its modification by $ZnCl_2$.

Performance of the prepared ZCPs

In order to enhance our adsorbents value, we carried out a comparative study of the maximum adsorption capacity obtained for the same pollutant to other adsorbents and activated carbons reported in the literature. Table 10 represents the different q_{max} values for BG adsorption by different adsorbents. It can be observed that the BG dye adsorption with ZCPs was obtained with acceptable values. The differences in the BG uptake values return to many factors such as the adsorbent structure, surface area, and the functional groups. ZCPs could be an attractive adsorbent for basic dyes owing to their isoelectric point pH_{pzc}.

Conclusion

Here, an investigation of the derived date pits' activated carbon usage for brilliant green removal was obtained. The following findings were obtained based on the experimental results from the current study:

(1) The prepared activated Carbons (CPs and ZCPs) were characterized by the BET, SEM, and FTIR techniques.
(2) The activated carbon SBET value increased with increasing the ZnCl2 impregnation ratio, it raised from 289.51 m^2/g for ZCP11 material to 667.89 m^2/g for ZCP31 material.
(3) The ZCPs efficiency was examined for the decolonization of BG; the influence of the solution's initial pH, dye (BG) concentration, contact time, adsorbent dose,

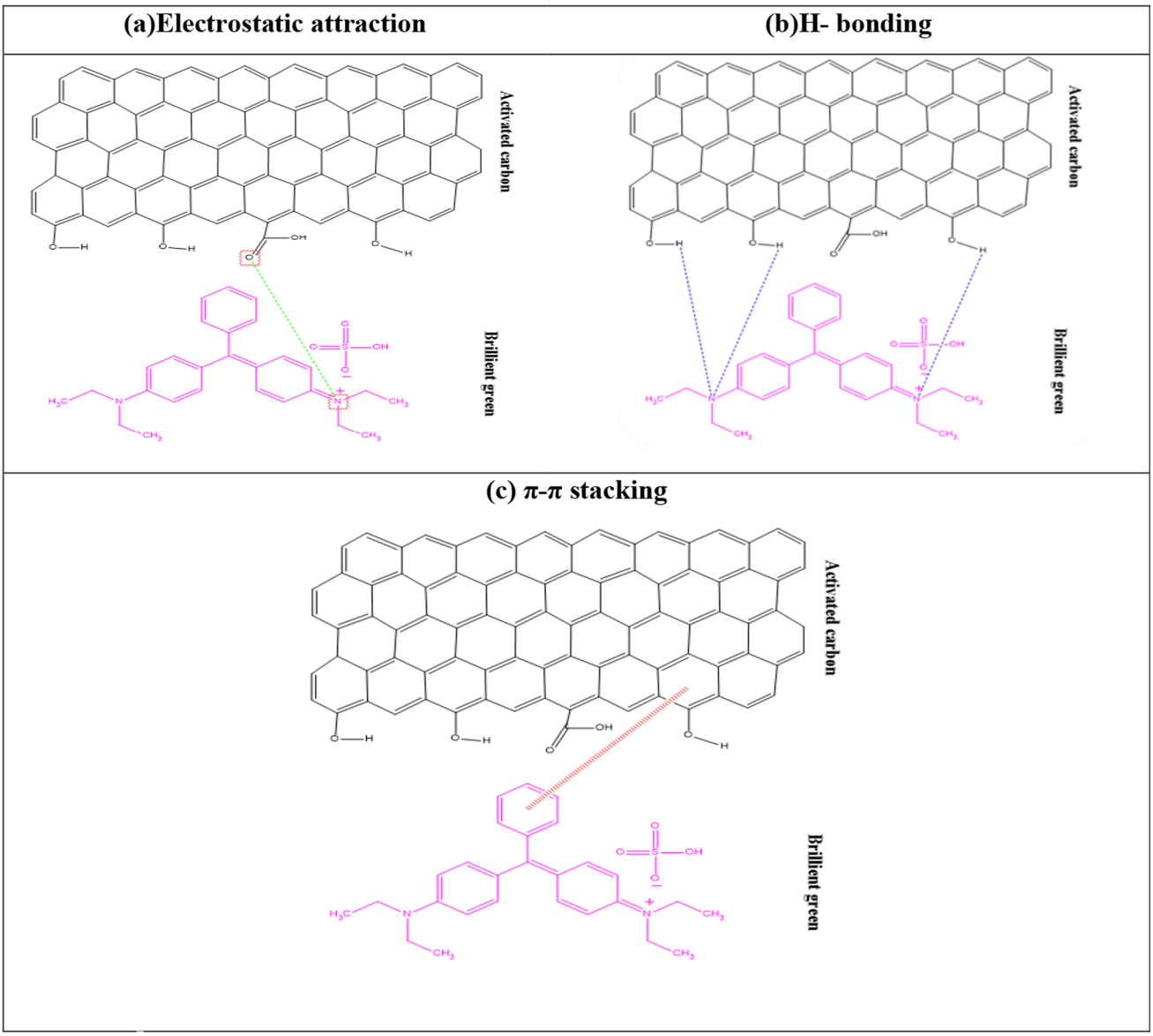

Fig. 14 Plausible mechanism of adsorption of BG onto ZCPs biosorbents

and temperature on the adsorption of BG was investigated.

(4) As the BG initial concentration increased, the ZCPs adsorption efficiency for BG increased, whereas the optimum shaking time and pH were shown to be 2 h and 7, respectively.

(5) The BG adsorption data are well matched with the Langmuir isothermal and the pseudo-2nd-order kinetic models.

(6) The BG adsorption onto ZCPs biosorbents is a spontaneous and endothermic process, based on negative ΔG^{o} and positive ΔH^{o} values. Meanwhile the positive ΔS^{o} value describes that the randomization increased at the solid (ZCPs)-liquid (BG solution) interface.

(7) The plausible mechanism of BG loading/adsorption onto the prepared ZCPs might be assigned to various interactions such as pore-filling, electrostatic attraction, H-bonding, and π–π. Figure 15 summaries the synthesis of ZCPs and their use for adsorption of BG.

Table 9 Recovery of BG from different water samples using unmodified carbon (CP) and zinc chloride activated carbon (ZCP31) ($n=5$)

Sample	Sorbent	Spiked (μg mL^{-1})	Measured (μg mL^{-1})	Recovered (μg mL^{-1})	Recovery (%)
Bidistilled water (Our lab)	CP	0.00	0.00	0.00	0.00
		5	1.05	3.95	79.0
		10	3.05	6.95	69.5
	ZCP31	0.00	0.00	0.00	0.00
		5.0	0.1	4.9	98.00
		10.0	0.8	9.2	92.0
Tab water (domestic supply))	CP	0.00	0.00	0.00	0.00
		5.00	0.9	4.1	82.00
		10.0	2.0	8.0	80.0
	ZCP31	0.00	0.00	0.00	0.00
		5.0	0. 2	4.8	96.00
		10.0	0.93	9.07	90.7
Waste water (Sewage drainage station- Ibb	CP	0.00	0.00	0.00	0.00
		5.0	1.33	3.67	73.4
		10.0	2.27	7.73	77.3
	ZCP31	0.00	0.00	0.00	0.00
		5.0	0.25	4.75	95.00
		10.0	0.96	9.04	90.04
Underground water (Ibb City)	CP	0.00	0.00	0.00	0.00
		5.0	1.4	3.6	72.0
		10.0	2.84	8.16	81.6
	ZCP31	0.00	0.00	0.00	0.00
		5.0	0. 4	4.6	92.0
		10.0	0.84	9.16	91.6

Table 10 Comparison of maximum sorption capacity of BG by proposed ZCP_S with some of the previously published articles

Adsorbents	Qm (mg/g)	References
Activated carbon prepared from cashew nut shell	243.90	(Samiyammal et al. 2022)
ZnS nanoparticles loaded activated carbon	258.7	(Jamshidi et al. 2016)
Activated carbon derived from guava tree wood	90	(Mansour et al. 2020)
Red clay	125	(Rehman et al. 2013)
Algerian montmorillonite	229	(Aichour and Zaghouane-Boudiaf 2019)
Saklikent mud	1.18	(Kismir and Aroguz 2011)
Modified chitosan	10.91	(Karaer and Uzun 2013)
Hydrogel Loaded with kalonite	26.31	(Shirsath et al. 2013)
Kaolin	65.42	(Nandi et al. 2009)
Yemen natural clay	476.4	(Nassar et al. 2012)
Nano Hydroxyapatite/Chitosan Composite	49.11	(Ragab et al. 2019)
Modified *Bambusa Tulda*	41.67	(Laskar and Kumar 2019)
Novel Acorn based adsorbent	2.11	(Ghaedi et al. 2011)
Activated carbon from Date Pits (CP)	74.98	*Current study*
Activated carbon from Date Pits (ZCP11)	192.02	*Current* study
Activated carbon from Date Pits (ZCP21)	201.02	*Current* study
Activated carbon from Date Pits (ZCP31)	247.75	*Current* study

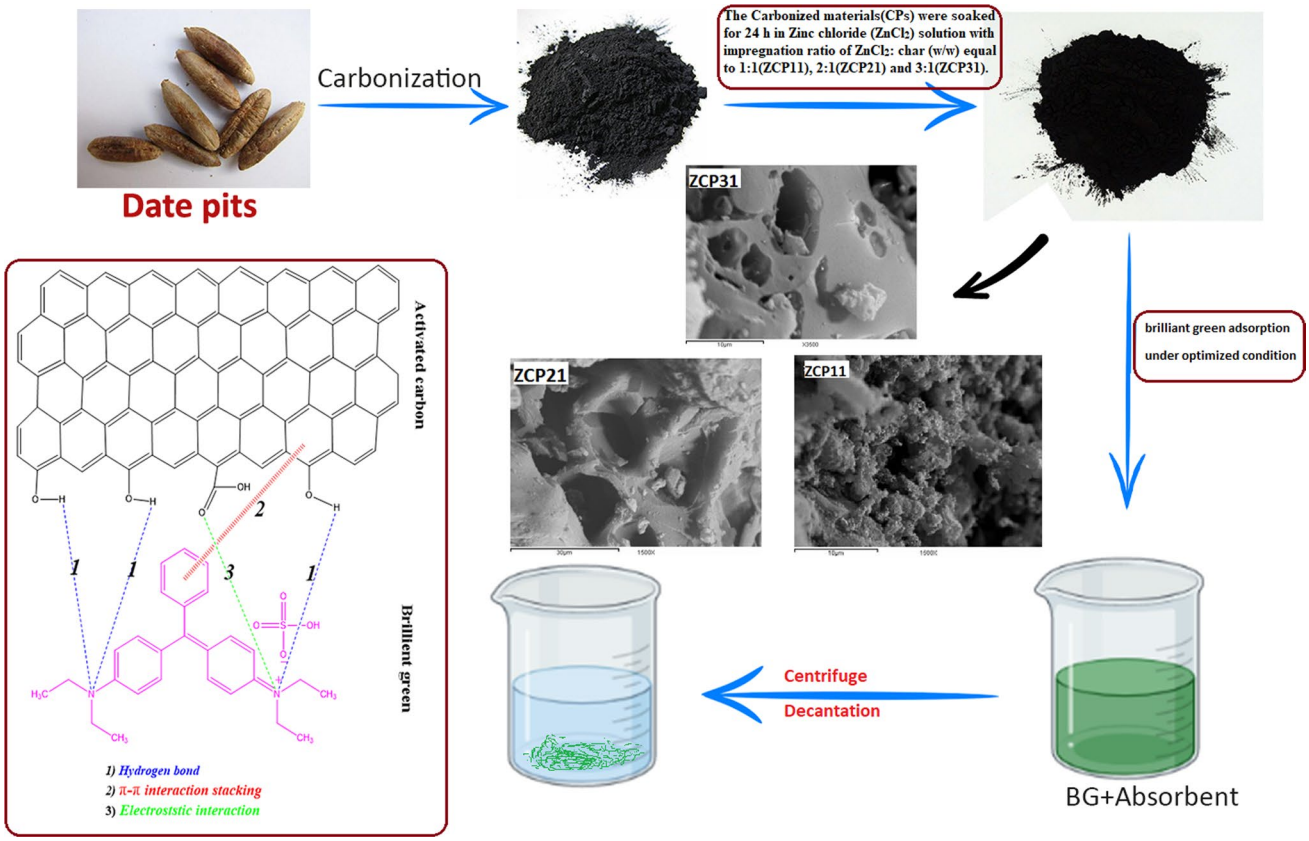

Fig. 15 Synthesis of ZCPs and its use for adsorption of BG

Acknowledgements Not applicable to this study.

Authors' contributions M A. Akl: Conceptualization, Methodology, Investigation, Writing—original draft, review. A.G Mostafa Writing—original draft, review. Mohammed M.H Al-Awadhi: Conceptualization, Writing—original draft, review. W.S Al-Harwi**:** Writing—original draft, review. Abdelrahman S El-Zeny: Writing—original draft, review.

Funding Open access funding provided by The Science, Technology & Innovation Funding Authority (STDF) in cooperation with The Egyptian Knowledge Bank (EKB). This research didn't receive external funding.

Data availability All data generated or analyzed during this study are included in this published article.

Declarations

Conflict of interests The authors declare that they have no competing interests".

Ethical approval and consent to participate Not applicable to this study.

Consent for publication Not applicable to this study.

References

Abdel-Fadeel MA, Aljohani NS, Al-Mhyawi SR, Halawani RF, Aljuhani EH, Salam MA (2022) A simple method for removal of toxic dyes such as Brilliant Green and Acid Red from the aquatic environment using Halloysite nanoclay. J Saudi Chem Soc 26(3):101475

Abd-Elhamid AI, Emran M, El-Sadek MH, El-Shanshory AA, Soliman HM, Akl MA, Rashad M (2020) Enhanced removal of cationic

dye by eco-friendly activated biochar derived from rice straw. Appl Water Sci 10:1–11
Aichour A, Zaghouane-Boudiaf H (2019) Highly brilliant green removal from wastewater by mesoporous adsorbents: kinetics, thermodynamics and equilibrium isotherm studies. Microchem J 146:1255–1262
Akl MA, Yousef AM, AbdElnasser S (2013) Removal of iron and manganese in water samples using activated carbon derived from local agro-residues. J Chem Eng Process Technol 4(4):1–10
Akl MA, El-Zeny AS, Hashem MA, El-Gharkawy ESR (2021) Synthesis, characterization and analytical applications of chemically modified cellulose for remediation of environmental pollutants. Egypt J Chem 64(7):3889–3901
Akl MA, Hashem MA, Ismail MA, Abdelgalil DA (2022b) Novel diaminoguanidine functionalized cellulose: synthesis, characterization, adsorption characteristics and application for ICP-AES determination of copper (II), mercury (II), lead (II) and cadmium (II) from aqueous solutions. BMC Chemistry 16(1):65
Akl MA, El-Zeny AS, Hashem MA, El-Gharkawy ESR, Mostafa AG (2023b) Flax fiber based semicarbazide biosorbent for removal of Cr (VI) and Alizarin Red S dye from wastewater. Sci Rep 13(1):8267
Akl MA, El-Zeny AS, Ismail M, Abdalla M, Abdelgelil D, Mostafa AG (2023c) Smart guanyl thiosemicarbazide functionalized dialdehyde cellulose for removal of heavy metal ions from aquatic solutions: adsorption characteristics and mechanism study. Appl Water Sci 13(6):1–18
Akl MA, Hashem MA, Mostafa AG (2022a) Synthesis, characterization, antimicrobial and photocatalytic properties of nano-silver-doped flax fibers. Polym Bull 80(9):9745–9777
Akl MA, El-Mahdy N, Al-Awadhi MM, Mostafa A (2023a) Cationic organo-montmorillonite for efficient concomitant removal of anionic dyes in single and multi-components' solutions: adsorption characteristics and mechanism study. Egypt J Chem. https://doi.org/10.21608/EJCHEM.2023.210347.7962
Al-Awadhi MH, Bashnaini M, Akl MA (2023) Biosorption of Lead (II) and Aluminum (III) from real water samples onto Precursor Pistachio shells: adsorption characteristics, kinetics and thermodynamic studies. Egypt J Chem 66(10):259–268
Al-Bowait M, Al-Sultan SI (2006) Aspects of the serum biochemistry, carcass quality and organoleptic characteristics of broilers fed alkali-treated date pits. Int J Poult Sci 5(3):284–288
Al-Farsi M, Alasalvar C, Al-Abid M, Al-Shoaily K, Al-Amry M, Al-Rawahy F (2007) Compositional and functional characteristics of dates, syrups, and their by-products. Food Chem 104(3):943–947
Almana HA, Mahmoud RM (1994) Palm date seeds as an alternative source of dietary fiber in Saudi bread. Ecol Food Nutr 32(3–4):261–270
Alvarez J, Lopez G, Amutio M, Bilbao J, Olazar M (2014) Bio-oil production from rice husk fast pyrolysis in a conical spouted bed reactor. Fuel 128:162–169
Ashraf Z, Hamidi-Esfahani Z (2011) Date and date processing: a review. Food Rev Intl 27(2):101–133
Aziz F, Rehman MS, Batool A, Muhammad A, Mahmood T (2012) Pretreatment of municipal, industrial and composite wastewater by ozonation. Environ Process Eng 1(2).
Bakr AA, Sayed NA, Salama TM, Ali IO, Gayed RA, Negm NA (2018) Kinetics and thermodynamics of Mn (II) removal from aqueous solutions onto Mg-Zn-Al LDH/montmorillonite nanocomposite. Egypt J Pet 27(4):1215–1220
Behera SS, Sourav D, Parhi PK, Tripathy SK, Mohapatra RK, Mayadhar D (2017) Kinetics, thermodynamics and isotherm studies on adsorption of methyl orange from aqueous solution using ion exchange resin Amberlite IRA-400. Desalin Water Treat 60:249–260
Besbes S, Blecker C, Deroanne C, Lognay G, Drira NE, Attia H (2005) Heating effects on some quality characteristics of date seed oil. Food Chem 91(3):469–476
Boehm HP (1994) Some aspects of the surface chemistry of carbon blacks and other carbons. Carbon 32(5):759–769
Brunauer S, Emmett PH, Teller E (1938) Adsorption of gases in multimolecular layers. J Am Chem Soc 60(2):309–319
Chang B, Guan D, Tian Y, Yang Z, Dong X (2013) Convenient synthesis of porous carbon nanospheres with tunable pore structure and excellent adsorption capacity. J Hazard Mater 262:256–264
Cheng S, Liu Y, Xing B, Qin X, Zhang C, Xia H (2021a) Lead and cadmium clean removal from wastewater by sustainable biochar derived from poplar saw dust. J Clean Prod 314:128074
Cheng S, Xing B, Shi C, Nie Y, Xia H (2021b) Efficient and selective removal of Pb (II) from aqueous solution by modification crofton weed: experiment and density functional theory calculation. J Clean Prod 280:124407
Cherifi H, Hanini S, Bentahar F (2009) Adsorption of phenol from wastewater using vegetal cords as a new adsorbent. Desalination 244(1–3):177–187
El Nemr A (2009) Potential of pomegranate husk carbon for Cr (VI) removal from wastewater: Kinetic and isotherm studies. J Hazard Mater 161(1):132–141
Faix O (1992) Fourier transform infrared spectroscopy. Methods in lignin chemistry. Springer, Berlin Heidelberg, Berlin, Heidelberg, pp 83–109
Ghaedi M, Hossainian H, Montazerozohori M, Shokrollahi A, Shojaipour F, Soylak MUSTAFA, Purkait MK (2011) A novel acorn based adsorbent for the removal of brilliant green. Desalination 281:226–233
Ghaedi M, Zeinali N, Ghaedi AM, Teimuori M, Tashkhourian J (2014) Artificial neural network-genetic algorithm based optimization for the adsorption of methylene blue and brilliant green from aqueous solution by graphite oxide nanoparticle. Spectrochim Acta Part A Mol Biomol Spectrosc 125:264–277
Gómez-Serrano V, Acedo-Ramos M, López-Peinado AJ, Valenzuela-Calahorro C (1994) Oxidation of activated carbon by hydrogen peroxide. Study of surface functional groups by FT-ir. Fuel 73(3):387–395
Goscianska J, Marciniak M, Pietrzak R (2014) Mesoporous carbons modified with lanthanum (III) chloride for methyl orange adsorption. Chem Eng J 247:258–264
Hai A, Bharath G, Babu KR, Taher H, Naushad M, Banat F (2019) Date seeds biomass-derived activated carbon for efficient removal of NaCl from saline solution. Process Saf Environ Prot 129:103–111
Hu Z, Srinivasan MP, Ni Y (2001) Novel activation process for preparing highly microporous and mesoporous activated carbons. Carbon 39(6):877–886
Húmpola P, Odetti H, Moreno-Piraján JC, Giraldo L (2016) Activated carbons obtained from agro-industrial waste: textural analysis and adsorption environmental pollutants. Adsorption 22:23–31
Ibrahim A, El Fawal GF, Akl MA (2019) Methylene blue and crystal violet dyes removal (as a binary system) from aqueous solution using local soil clay: kinetics study and equilibrium isotherms. Egypt J Chem 62(3):541–554
Idrees M, Batool S, Kalsoom T, Yasmeen S, Kalsoom A, Raina S, Kong J (2018) Animal manure-derived biochars produced via fast pyrolysis for the removal of divalent copper from aqueous media. J Environ Manag 213:109–118
Ioannidou O, Zabaniotou A (2007) Agricultural residues as precursors for activated carbon production—A review. Renew Sustain Energy Rev 11(9):1966–2005
Islam MA, Ahmed MJ, Khanday WA, Asif M, Hameed BH (2017) Mesoporous activated carbon prepared from NaOH activation of rattan (Lacosperma secundiflorum) hydrochar for methylene blue removal. Ecotoxicol Environ Saf 138:279–285

Jamshidi M, Ghaedi M, Dashtian K, Ghaedi AM, Hajati S, Goudarzi A, Alipanahpour E (2016) Highly efficient simultaneous ultrasonic assisted adsorption of brilliant green and eosin B onto ZnS nanoparticles loaded activated carbon: artificial neural network modeling and central composite design optimization. Spectrochim Acta Part A Mol Biomol Spectrosc 153:257–267

Javaid M, Saleemi AR, Naveed S, Zafar M, Ramzan N (2011) Anaerobic treatment of desizing effluent in a mesophilic anaerobic packed bed reactor. JPIChE 39(61):e67

Jia YF, Xiao B, Thomas KM (2002) Adsorption of metal ions on nitrogen surface functional groups in activated carbons. Langmuir 18(2):470–478

Karaer H, Uzun I (2013) Adsorption of basic dyestuffs from aqueous solution by modified chitosan. Desalin Water Treat 51(10–12):2294–2305

Kennedy LJ, Vijaya JJ, Sekaran G (2004) Effect of two-stage process on the preparation and characterization of porous carbon composite from rice husk by phosphoric acid activation. Ind Eng Chem Res 43(8):1832–1838

Kennedy LJ, Vijaya JJ, Sekaran G (2005) Electrical conductivity study of porous carbon composite derived from rice husk. Mater Chem Phys 91(2–3):471–476

Kismir Y, Aroguz AZ (2011) Adsorption characteristics of the hazardous dye Brilliant Green on Saklıkent mud. Chem Eng J 172(1):199–206

Kumar CG, Mongolla P, Joseph J, Sarma VUM (2012) Decolorization and biodegradation of triphenylmethane dye, brilliant green, by Aspergillus sp. isolated from Ladakh India. Process Biochem 47(9):1388–1394

Kumar R, Ansari MO, Barakat MA (2014) Adsorption of brilliant green by surfactant doped polyaniline/MWCNTs composite: evaluation of the kinetic, thermodynamic, and isotherm. Ind Eng Chem Res 53(17):7167–7175

Kurt E, Koseoglu-Imer DY, Dizge N, Chellam S, Koyuncu I (2012) Pilot-scale evaluation of nanofiltration and reverse osmosis for process reuse of segregated textile dyewash wastewater. Desalination 302:24–32

Lam SS, Liew RK, Cheng CK, Rasit N, Ooi CK, Ma NL, Chase HA (2018) Pyrolysis production of fruit peel biochar for potential use in treatment of palm oil mill effluent. J Environ Manag 213:400–408

Laskar N, Kumar U (2019) Removal of Brilliant Green dye from water by modified Bambusa Tulda: adsorption isotherm, kinetics and thermodynamics study. Int J Environ Sci Technol 16:1649–1662

Litefti K, Freire MS, Stitou M, González-Álvarez J (2019) Adsorption of an anionic dye (Congo red) from aqueous solutions by pine bark. Sci Rep 9(1):16530

Lotito AM, Fratino U, Bergna G, Di Iaconi C (2012) Integrated biological and ozone treatment of printing textile wastewater. Chem Eng J 195:261–269

Mahdi Z, Hanandeh AE, Yu Q (2017) Influence of pyrolysis conditions on surface characteristics and methylene blue adsorption of biochar derived from date seed biomass. Waste Biomass Valorization 8:2061–2073

Mahdi Z, Yu QJ, El Hanandeh A (2018) Investigation of the kinetics and mechanisms of nickel and copper ions adsorption from aqueous solutions by date seed derived biochar. J Environ Chem Eng 6(1):1171–1181

Mansour RA, El Shahawy A, Attia A, Beheary MS (2020) Brilliant green dye biosorption using activated carbon derived from guava tree wood. Int J Chem Eng 2020:1–12

Meng J, Liang S, Tao M, Liu X, Brookes PC, Xu J (2018) Chemical speciation and risk assessment of Cu and Zn in biochars derived from co-pyrolysis of pig manure with rice straw. Chemosphere 200:344–350

Mittal H, Parashar V, Mishra SB, Mishra AK (2014) Fe3O4 MNPs and gum xanthan based hydrogels nanocomposites for the efficient capture of malachite green from aqueous solution. Chem Eng J 255:471–482

Mittal H, Maity A, Ray SS (2015) Synthesis of co-polymer-grafted gum karaya and silica hybrid organic–inorganic hydrogel nanocomposite for the highly effective removal of methylene blue. Chem Eng J 279:166–179

Mostafa AG, El-Mekabaty A, Hashem MA, Akl M (2021) Selective Separation of Cu (II) from a single metal ion solution by using O-amino thiophenol-modified flax fiberd. Egypt J Chem 64(4):1701–1708

Mostafa AG, Abd El-Hamid AI, Akl MA (2023) Surfactant-supported organoclay for removal of anionic food dyes in batch and column modes: adsorption characteristics and mechanism study. Appl Water Sci 13(8):163

Murmu BM, Behera SS, Das S, Mohapatra RK, Parhi P (2019) Extensive investigation on the study for the adsorption of Bromocresol Green (BCG) dye using activated Phragmites karka. Ind J Chem Technol (IJCT) 25(5):409–420

Nandi BK, Goswami A, Purkait MK (2009) Adsorption characteristics of brilliant green dye on kaolin. J Hazard Mater 161(1):387–395

Nassar MM, El-Geundi MS, Al-Wahbi AA (2012) Equilibrium modeling and thermodynamic parameters for adsorption of cationic dyes onto Yemen natural clay. Desalin Water Treat 44(1–3):340–349

Omrani N, Nezamzadeh-Ejhieh A (2020) Focus on scavengers' effects and GC-MASS analysis of photodegradation intermediates of sulfasalazine by Cu2O/CdS nanocomposite. Sep Purif Technol 235:116228

Qi L, Xu Z (2004) Lead sorption from aqueous solutions on chitosan nanoparticles. Colloids Surf, A 251(1–3):183–190

Qian F, Sun X, Liu Y (2013) Removal characteristics of organics in bio-treated textile wastewater reclamation by a stepwise coagulation and intermediate GAC/O3 oxidation process. Chem Eng J 214:112–118

Ragab A, Ahmed I, Bader D (2019) The removal of brilliant green dye from aqueous solution using nano hydroxyapatite/chitosan composite as a sorbent. Molecules 24(5):847

Rehman MSU, Kim I, Han JI (2012) Adsorption of methylene blue dye from aqueous solution by sugar extracted spent rice biomass. Carbohyd Polym 90(3):1314–1322

Rehman MSU, Munir M, Ashfaq M, Rashid N, Nazar MF, Danish M, Han JI (2013) Adsorption of Brilliant Green dye from aqueous solution onto red clay. Chem Eng J 228:54–62

Sahari MA, Barzegar M, Radfar R (2007) Effect of varieties on the composition of dates (*Phoenix dactylifera* L.)—note. Food Sci Technol Int 13(4):269–275

Sain M, Panthapulakkal S (2006) Bioprocess preparation of wheat straw fibers and their characterization. Ind Crops Prod 23(1):1–8

Samiyammal P, Kokila A, Pragasan LA, Rajagopal R, Sathya R, Ragupathy S, Reddy VRM (2022) Adsorption of brilliant green dye onto activated carbon prepared from cashew nut shell by KOH activation: studies on equilibrium isotherm. Environ Res 212:113497

Serage AA, Mostafa MM, Akl MA (2022) Low cost agro-residue derived biosorbents: synthesis, characterization and application for removal of lead ions from aqueous solutions. Egypt J Chem 65(131):447–461

Shi LE, Zheng W, Aleid SM, Tang ZX (2014) Date pits: chemical composition, nutritional and medicinal values, utilization. Crop Sci 54(4):1322–1330

Shirsath SR, Patil AP, Patil R, Naik JB, Gogate PR, Sonawane SH (2013) Removal of Brilliant Green from wastewater using conventional and ultrasonically prepared poly (acrylic acid) hydrogel

loaded with kaolin clay: a comparative study. Ultrason Sonochem 20(3):914–923
Southichak B, Nakano K, Nomura M, Chiba N, Nishimura O (2006) Phragmites australis: a novel biosorbent for the removal of heavy metals from aqueous solution. Water Res 40(12):2295–2302
Sun L, Tian C, Li M, Meng X, Wang L, Wang R, Fu H (2013) From coconut shell to porous graphene-like nanosheets for high-power supercapacitors. J Mater Chem A 1(21):6462–6470
Tan IAW, Ahmad AL, Hameed DB (2008) Preparation of activated carbon from coconut husk: optimization study on removal of 2, 4, 6-trichlorophenol using response surface methodology. J Hazard Mater 153(1–2):709–717
Tang ZX, Shi LE, Aleid SM (2013) Date fruit: chemical composition, nutritional and medicinal values, products. J Sci Food Agric 93(10):2351–2361
Tang Q, Shi C, Shi W, Huang X, Ye Y, Jiang W, Li D (2019) Preferable phosphate removal by nano-La (III) hydroxides modified mesoporous rice husk biochars: role of the host pore structure and point of zero charge. Sci Total Environ 662:511–520
Youssef AM, Alaya MN, Nawar N (1994) Adsorption properties of activated carbons obtained from polymer wastes. Adsorpt Sci Technol 11(4):225–233
Youssef NA, Shaban SA, Ibrahim FA, Mahmoud AS (2016) Degradation of methyl orange using Fenton catalytic reaction. Egypt J Pet 25(3):317–321
Yue Z, Mangun CL, Economy J (2002) Preparation of fibrous porous materials by chemical activation: 1. ZnCl2 activation of polymer-coated fibers. Carbon 40(8):1181–1191
Zhang L, Zhou X, Guo X, Song X, Liu X (2011) Investigation on the degradation of acid fuchsin induced oxidation by MgFe2O4 under microwave irradiation. J Mol Catal a: Chem 335(1–2):31–37